



# Diffusion of gold ions and gold particles during photoreduction processes probed by the transient grating method

Masafumi Harada<sup>a,\*</sup>, Koichi Okamoto<sup>b</sup>, Masahide Terazima<sup>c</sup>

<sup>a</sup> Department of Health Science and Clothing Environment, Faculty of Human Life and Environment, Nara Women's University, Nara 630-8506, Japan

<sup>b</sup> Department of Electronic Science and Engineering, Graduate School of Engineering, Kyoto University, Kyoto 615-8510, Japan

<sup>c</sup> Department of Chemistry, Graduate School of Science, Kyoto University, Kyoto 606-8502, Japan

## ARTICLE INFO

### Article history:

Received 17 September 2008

Accepted 17 December 2008

Available online 24 December 2008

### Keywords:

Colloidal dispersions

Gold ions

Gold particles

Photoreduction

Laser induced transient grating method

## ABSTRACT

The translational diffusion of Au (gold) ions and Au particles during the photoreduction process from  $\text{AuCl}_4^-$  to metallic Au particles in aqueous ethanol solutions containing poly(*N*-vinyl-2-pyrrolidone) was investigated by using UV–vis absorption and the laser-induced transient grating (TG) methods. The TG signal of  $\text{AuCl}_4^-$  solution before photoirradiation was composed of three contributions; the thermal grating, the species grating due to the creation of  $\text{AuCl}_2^-$ , and that due to the depletion of  $\text{AuCl}_4^-$ . Upon photoirradiation, the species grating signal due to  $\text{AuCl}_4^-$  diminished rapidly and the TG signal due to Au particles appeared within a few minutes and became stronger at a very short time. The subsequent reduction of  $\text{AuCl}_2^-$  was concomitant with the formation of Au metal particles. The rapid growth of  $\text{Au}^0$  atoms into Au particles took place in the short-duration photoirradiation. With the increase of the photoirradiation time, the TG signal was composed of two kinds of Au particle fragments possessing different diffusion coefficients. This is probably due to the pulse-laser induced fragmentation of the larger Au particles. Effects of the polymer on the particle formation were investigated by the concentration dependence of the polymer in the solution. The formation of Au particles by the photoreduction was also compared with that of Pt particles.

© 2009 Elsevier Inc. All rights reserved.

## 1. Introduction

Nanoparticles exhibit a variety of size-dependent optical and electrical properties which could be used in a variety of technologies, including coating, environmental, chemical processes, medical, electronic and sensing applications [1–3]. In order to effectively utilize their size-dependent properties, the size and polydispersity have to be controlled. For this purpose, organic stabilization ligands are often used such as polymer [4–7], surfactant [8,9], dendrimer [10], alkanethiol [11], alkylamine [12] and so on.

For the preparation of metal nanoparticles, metal ions have often been reduced in various solutions of polymers and surfactants. As protective media for metal particles in solutions, water-soluble polymers such as poly(vinyl alcohol) (PVA) [4], poly(*N*-vinyl-2-pyrrolidone) (PVP) [5], polyacrylate [6], and polystyrene-poly-4-vinylpyridine block copolymer (PS-*b*-P4VP) [7] have often been used. In particular, optical properties of gold, silver, and copper have been extensively studied since they strongly absorb light in the visible region due to surface plasma resonance. The reduction of gold ions can be achieved chemically, for example, by

using sodium borohydride [13] and hydrazine [14], sonochemically [15], electrochemically [16], or radiolytically (by using  $\gamma$ -irradiation [4,6,17], UV-irradiation [18], and so on).

Laser-induced transient grating (TG) technique [19] is one of powerful methods to study photo-induced reactions, such as the diffusion processes of short-lived radicals [20], intermediates of protein reactions [21,22], or carrier diffusion in semiconductors [23,24]. Recently, we investigated the formation of Pt particles during the photoirradiation in the PVP solutions by means of the TG method [25]. It was found that the transformation of  $\text{PtCl}_6^{2-}$  to  $\text{PtCl}_4^{2-}$  species completed within a few minutes after photoirradiation.  $\text{PtCl}_4^{2-}$  was much more stable than  $\text{PtCl}_6^{2-}$  in the aqueous solutions under the photoirradiation. The created  $\text{PtCl}_4^{2-}$  was gradually reduced to  $\text{Pt}^0$  atoms during a long-duration photoirradiation, and concurrently the increasing number of Pt particles associated from the  $\text{Pt}^0$  atoms was observed during the photoirradiation.

In this paper, we report the process of Au particle formation from  $\text{AuCl}_4^-$  solution by the UV–vis absorption and the TG techniques. Recently, one of authors has investigated the photoreduction of  $\text{AuCl}_4^-$  to metallic Au particles by means of XAFS measurements [26]. From the XANES analysis, the electronic structure of the photoirradiated samples was elucidated to be composed of

\* Corresponding author. Fax: +81 742 20 3466.

E-mail address: harada@cc.nara-wu.ac.jp (M. Harada).

three stable electronic states,  $\text{Au}^{3+}$  (that is a reactant,  $\text{AuCl}_4^-$ ),  $\text{Au}^+$  (that is stable intermediate product,  $\text{AuCl}_2^-$ ), and Au particle produced from  $\text{Au}^0$  atoms. In this photoreduction process, the reduction of  $\text{AuCl}_2^-$  to  $\text{Au}^0$  atoms is a slower process than that of  $\text{AuCl}_4^-$  to  $\text{AuCl}_2^-$ , and the reduction of  $\text{AuCl}_2^-$  to  $\text{Au}^0$  atoms and the association of  $\text{Au}^0$  atoms to form seed Au particles (particle diameter between 5.5 and 30 Å) concurrently proceeds in the short-duration photoirradiation. In addition, on the long-duration photoirradiation, the slow progress of Au particle growth occurs with the association of  $\text{Au}^0$ – $\text{Au}^0$  metallic bonds, resulting in the formation of larger Au particle (particle diameter larger than 500 Å) [26].

In order to study the mechanism of reduction of  $\text{AuCl}_4^-$  to  $\text{Au}^0$  atoms and association of  $\text{Au}^0$  atoms to create larger Au particles in more detail, we have carefully compared the previous XAFS results with the present TG results. Especially, the intermediate chemical species in the photoreduction process to create larger Au particles have been examined. We have also compared the present results with the previous ones of the photoreduction of Pt ions in PVP solution.

## 2. Principles

By the spatially modulated light due to the interference between two light beams, chemical species in a sample are excited to excited states in which photochemical reductions take place. Since the created species usually have different optical properties (such as absorption coefficients and refractive indices), the spatially modulated photoexcitation induces a spatially modulated absorbance (amplitude grating) or refractive index (phase grating) at the probe beam wavelength. The refractive index ( $n$ ) and absorbance ( $k$ ) in the sample solution after the excitation are represented by

$$n(x, t) = n_0 + \delta n_p(x, t) - \delta n_r(x, t) + \delta n_{th}(x, t), \quad (1)$$

$$k(x, t) = k_0 + \delta k_p(x, t) - \delta k_r(x, t), \quad (2)$$

where  $n_0$  and  $k_0$  are, respectively, the unperturbed refractive index and absorbance of the solution. The contribution of  $\delta n_{th}(x, t)$  represents the refractive index change ( $\delta n$ ) by the thermal expansion of the solution due to the radiationless transition from the excited state (thermal grating). The terms of  $\delta n_p(x, t)$  and  $\delta n_r(x, t)$  represent  $\delta n$  by the spatially modulated distribution of the product and the reactant, respectively. The  $\delta k_p(x, t)$  and  $\delta k_r(x, t)$  terms in Eq. (2) represent the absorption change ( $\delta k$ ) due to the creation of the product and depletion of the reactant, respectively. By solving the diffusion rate equations, we can obtain the following equations, which display the time dependence of the spatial modulations [19,20,27]:

$$\delta n_{th}(q, t) = \delta n_{th}^0 \exp(-D_{th}q^2t), \quad (3)$$

$$\delta n_p(q, t) = \delta n_p^0 \exp(-D_pq^2t), \quad (4)$$

$$\delta n_r(q, t) = \delta n_r^0 \exp(-D_rq^2t), \quad (5)$$

$$\delta k_p(q, t) = \delta k_p^0 \exp(-D_pq^2t), \quad (6)$$

$$\delta k_r(q, t) = \delta k_r^0 \exp(-D_rq^2t), \quad (7)$$

where  $q$  is the grating wavenumber,  $D_{th}$  is the thermal diffusivity,  $D_p$  and  $D_r$  are the diffusion coefficients of the product and the reactant, respectively. Since the refractive index decreases with increasing temperature,  $\delta n_{th}^0$  should be negative. Under the thick grating and the weak diffraction conditions, the TG signal intensity  $I_{TG}(t)$  at grating wavenumber  $q$  is represented by

$$I_{TG}(t) = A(\delta n_{th}(q, t) + \delta n_p(q, t) - \delta n_r(q, t))^2 + B(\delta k_p(q, t) - \delta k_r(q, t))^2, \quad (8)$$

where  $A$  and  $B$  are constants.

## 3. Experimental

### 3.1. Materials

Colloidal dispersions of Au particles were synthesized by the photoreduction of  $\text{AuCl}_4^-$  with the protective polymer PVP. The average molecular weight of PVP used here was 40,000. Tetrachloroauric(III) acid (hydrogen tetrachloroaurate(III),  $\text{HAuCl}_4 \cdot 4\text{H}_2\text{O}$ ; guaranteed reagent), PVP (K-30), ethanol (guaranteed reagent, 99.5%), and distilled water were purchased from Nacalai Tesque, and gold(I) chloride ( $\text{AuCl}$ ) was obtained from Aldrich. They were used without further purification.

### 3.2. TG measurements

The setup of the TG method has been reported in detail elsewhere [19,20,22,24,25]. An excitation beam from an excimer laser [XeCl (308 nm), Lumonics Hyper-400] was split into two beams by a beam splitter. The repetition rate of the excitation pulse was 1–3 Hz, and the pulse width was about 20 ns. These beams were crossed inside a quartz sample cell (10 mm optical path length), and the interference pattern between these beams (optical grating) was created. The laser fluence at the crossing point was measured by a pyroelectric joulemeter (Molelectron J3-09), and it was typically  $\sim 0.3 \text{ mJ/cm}^2$ . The thermal energy released by the non-radiative relaxation raised the temperature of the sample, and it created the thermal grating. The excited ions partly reacted, and the concentrations of the reactant and product were modulated (species grating). A He–Ne laser was used as a probe beam and brought into the crossing region at the Bragg angle. A diffracted probe beam (the TG signal) was isolated from the excitation beams with a pinhole and a red filter (Toshiba R-60) with a cutoff wavelength of 600 nm. The intensity of the TG signal was detected by a photomultiplier tube (Hamamatsu R-928) and recorded with a digital oscilloscope (Tektronix 2430A). The fringe spacing  $\Lambda$  was calculated from the decay rate of the thermal grating signal of a benzene solution [27].

Colloidal dispersions of Au particles (0.66 mM) were prepared from  $\text{HAuCl}_4 \cdot 4\text{H}_2\text{O}$  by irradiation with a 500 W super-high-pressure mercury lamp in a solution of water and ethanol (the volume ratio of water and ethanol is 1/1) containing PVP. The concentration of polymer in water/ethanol (1/1) solutions was varied at  $[\text{PVP monomeric unit}]/[\text{metal}] = 4$  and 400, which we call dilute and concentrated polymer solutions, respectively. Briefly, for the preparation of the dilute polymer solution, 5 mL of a 1.32 mM aqueous solution of  $\text{HAuCl}_4 \cdot 4\text{H}_2\text{O}$  was added to 5 mL of a 5.28 mM ethanol solution of PVP.  $\text{N}_2$  gas was bubbled into the solution, and vigorous stirring with a magnetic stirrer was carried out for 10 min to remove the dissolved  $\text{O}_2$ . For the preparation of the concentrated polymer solution, 5 mL of a 1.32 mM aqueous solution of  $\text{HAuCl}_4 \cdot 4\text{H}_2\text{O}$  was added to 5 mL of a 528 mM ethanol solution of PVP, followed by  $\text{N}_2$  bubbling and vigorous stirring. The ionic solutions were poured into a quartz sample cell, and were photoirradiated by the 500 W super-high-pressure mercury lamp.

Diffusion coefficients ( $D$ ) of Au ionic species and Au particles of the photoirradiated samples at the designated duration of reduction time were measured by the TG method. The direction of the photoirradiation using a mercury lamp was perpendicular to that for the TG measurement. The UV–vis absorption spectra of the pre-reduced (before irradiation) and the reduced (after irradiation for about 15 min) samples were measured with a Hitachi U-3010 spectrophotometer by using quartz cells (1 mm optical path length) to adjust the metal concentration for the UV measurements.

### 3.3. Characterization of Au particles

Transmission electron microscopy (TEM) images of the colloidal dispersions of Au particles were obtained using a JEM-2000FX in-

strument operated at 200 kV as the acceleration voltage. A high-resolution carbon-supported copper mesh was used to support the samples of colloidal dispersions. The diameter of each particle was determined from enlarged photographs. The particle size distribution and the average diameter were obtained by measuring about 200 particles in arbitrarily chosen areas in the enlarged photograph.

## 4. Results and discussion

### 4.1. Photochemical formation of Au particles from $\text{AuCl}_4^-$ in dilute PVP solution

The absorption spectrum of  $\text{AuCl}_4^-$  displayed an absorption band around 320 nm. This is attributed to the ligand-to-metal charge transfer (LMCT) [28]. Photoirradiation for the LMCT bands of  $\text{AuCl}_4^-$  complex in alcohol–water solution resulted in the reduction of  $\text{Au}^{3+}$  to  $\text{Au}^0$  particles with the simultaneous oxidation of the alcohol [4]. This process can be visually monitored by the color changes in the solution. The precursor solution of the  $\text{AuCl}_4^-$  was yellow in color before the photoirradiation. Within a few minutes after the photoirradiation, the color of the solution gradually turned purple, implying the formation of the intermediate species ( $\text{AuCl}_2^-$ ) [29]. After the photoirradiation longer than 30 min, the intermediate species were transformed to metallic  $\text{Au}^0$  particles, resulting in the color change of the solution from purple to red.

UV–vis measurements confirmed the reduction of  $\text{Au}^{3+}$  by the photoirradiation. Figs. 1a and 1b show the UV–vis absorption spectra of the Au-containing solutions with and without the polymer before and after the photoirradiation in the dilute and concentrated PVP solutions, respectively. The photoirradiation was performed for 15 min to check the formation of Au particles in solutions. The LMCT band disappeared immediately after the photoirradiation for 1–2 min, although no significant increase of the baseline in absorbance was observed at less than 1 min. This spectral change indicated that the reduction of  $\text{Au}^{3+}$  rapidly occurred under our conditions. Then, the surface plasmon absorption band at 550 nm appeared, and its intensity gradually became higher until the irradiation time of 15 min, indicating the formation of spherical Au particles in colloidal solution. By increasing the irradiation time beyond 15 min, the peak position of the plasmon absorption band did not change, and the red shift and broadening of the plasmon band was not observed. This result showed the aggregation of Au particles did not noticeably occur. The resulting solution was red in color and very dispersive at least several months. PVP was necessary for the stabilization of the Au colloidal particles, because the absence of the protective polymer caused the deposition of Au particles on the quartz cell.

Fig. 2, a to l, shows the time evolution of typical temporal profiles of the TG signals ( $I_{\text{TC}}$ ) before and after the photoirradiation by the mercury lamp for the dilute PVP solution of  $\text{Au}^{3+}$ . The signal obtained from the sample before photoirradiation is composed of three components, a spike-like signal, a subsequent slow rise, and a slow decay component, as shown in Fig. 2a. The spike-like signal, which decays in a few microseconds, originates from the thermal grating. After the thermal grating signal decays, the rise and slow decay components appear. Since these slow processes have time constants almost 2–3 orders of magnitude slower than that of the thermal grating, the time evolutions of these components must reflect the molecular diffusion in solutions.

The absorption of  $\text{Au}^{3+}$  is nearly zero at the wavelength of the probe beam (633 nm) as shown in Figs. 1a and 1b. Since the absorption of  $\text{Au}^{3+}$  is very weak at the probe wavelength, the am-

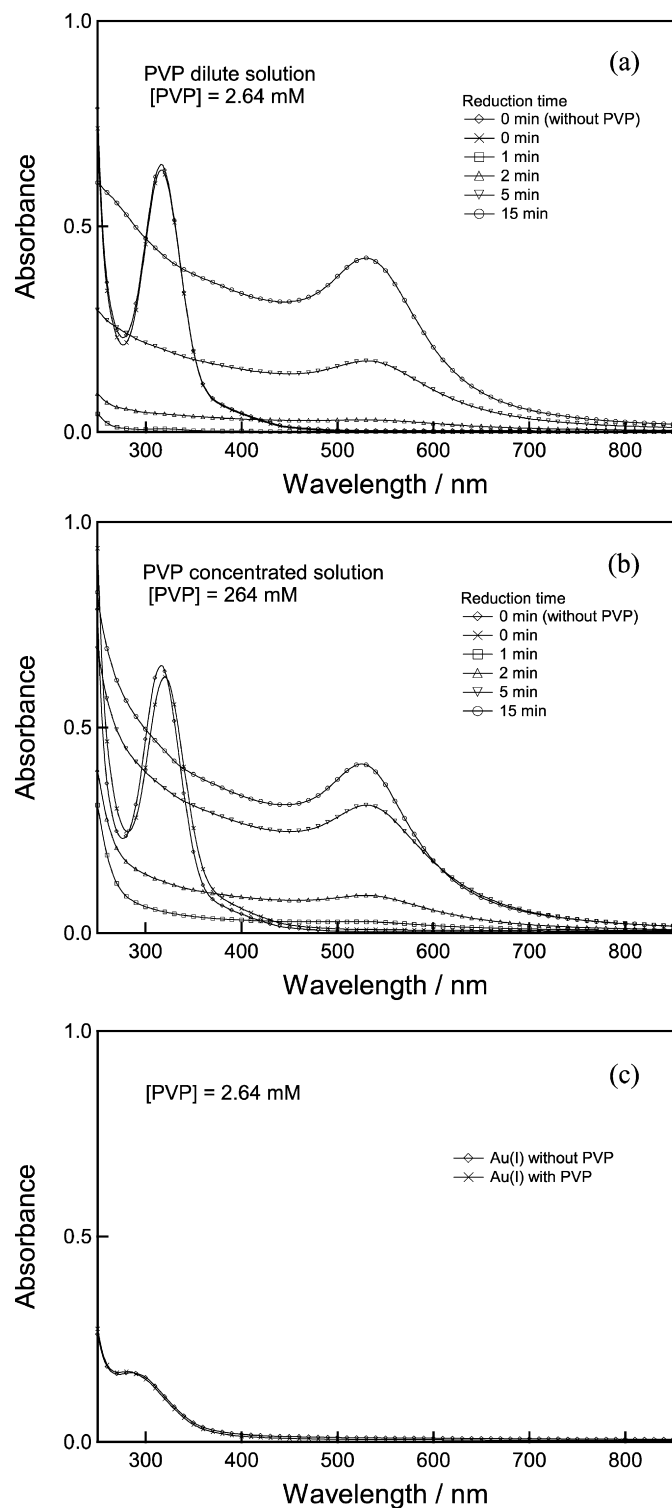


**Fig. 1.** UV–vis absorption spectra of the Au-containing solution (ethanol–water, 1:1 (v/v)) before and after the photoirradiation: (a)  $\text{HAuCl}_4 \cdot 4\text{H}_2\text{O}$  in the dilute PVP solution; (b)  $\text{HAuCl}_4 \cdot 4\text{H}_2\text{O}$  in the concentrated PVP solution; (c)  $\text{AuCl}$  solution with and without PVP. The photoreduction was carried out during 15 min. The spectrum of  $\text{HAuCl}_4 \cdot 4\text{H}_2\text{O}$ -containing solutions without PVP is also indicated.

plitude of the thermal grating in Eq. (8) can be neglected. Therefore, the TG signal ( $I_{\text{TC}}(t)$ ) before photoirradiation is predicted to be expressed by

$$I_{\text{TC}}(t) = A \left[ \delta n_{\text{th}}^0 \exp(-D_{\text{th}} q^2 t) + a_1 \exp(-k_1 t) + a_2 \exp(-k_2 t) \right]^2, \quad (9)$$

where  $a_1$  and  $a_2$  are the pre-exponential factors, and  $k_1$  and  $k_2$  are the decay rate constants of each component ( $k_1 > k_2$ ). As is

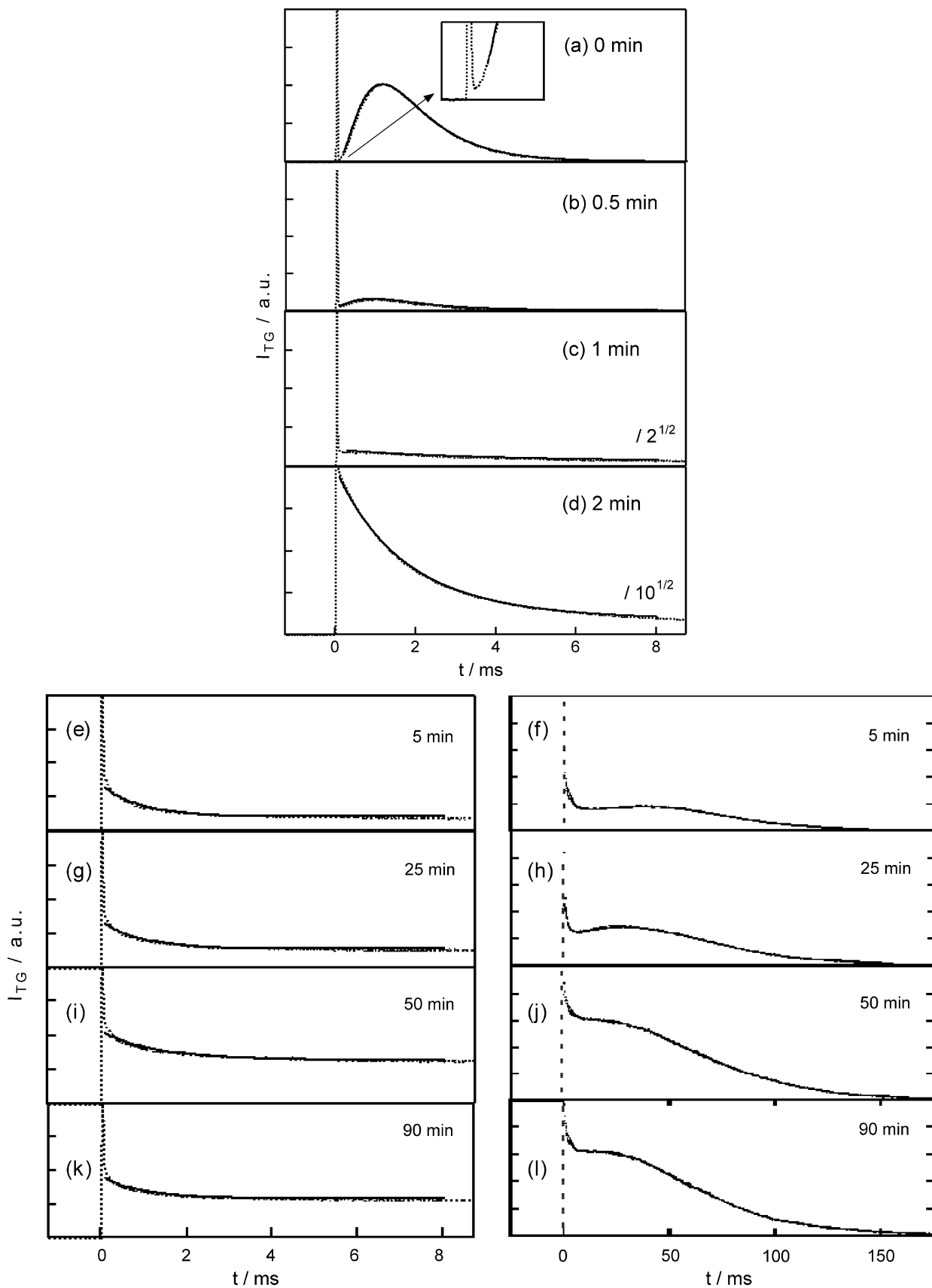


**Fig. 2.** Time dependence of the TG signals ( $I_{TG}$ ) in water/ethanol (1/1) solutions with PVP observed (a) before and (b to l) after the photoirradiation. The initial sharp spike-like signal is due to the contribution of the thermal grating. In all the cases, the best-fitted curves are drawn by solid line using by (a, b) Eq. (10) and (c to l) Eq. (11) after the decay of the thermal grating signal (dashed line). The concentration of polymer was at  $[\text{PVP monomeric unit}]/[\text{metal}] = 4$  (the dilute PVP solution). Inset figure indicates that the thermal grating signal do not decay to the baseline before the photoirradiation.

seen in the inset of Fig. 2a, the thermal grating signal do not decay to the baseline. Since the refractive index change ( $\delta n_{\text{th}}^0$ ) by the thermal expansion is negative, we can find out the signs of these components as  $a_1 > 0$  and  $a_2 < 0$ .

In the early stage of photochemical reduction process, chemical species such as  $\text{Au}^{3+}$ ,  $\text{Au}^{2+}$ ,  $\text{Au}^+$ , and  $\text{Au}^0$  would be possibly contributed to the signal. According to the previous studies [4,30],  $\text{Au}^{3+}$  and  $\text{Au}^+$  ionic species are more stable than  $\text{Au}^{2+}$  and  $\text{Au}^0$ . The very unstable  $\text{Au}^{2+}$  may undergo intramolecular reduction, producing one more  $\text{Cl}^-$  radical, or they may undergo disproportionation to  $\text{Au}^{3+}$  and  $\text{Au}^+$  species. Therefore, it is reasonable to consider that the slow decay components dominantly reflect the diffusion of the stable species such as  $\text{Au}^{3+}$  and  $\text{Au}^+$ .

On the basis of the Kramers–Kronig relation and the absorption bands in Fig. 1, both of  $\delta n_{\text{Au}^+}^0$  and  $\delta n_{\text{Au}^{3+}}^0$  should be positive because these chemical species possess absorption bands (286 nm and 320 nm, as shown in Figs. 1c and 1a, respectively) in the wavelength shorter than 633 nm. Hence, considering the signs of  $a_1 > 0$  and  $a_2 < 0$  of Eq. (9), we can conclude that the  $a_1 \exp(-k_1 t)$  and  $a_2 \exp(-k_2 t)$  terms should correspond to the  $\delta n_{\text{Au}^+}^0 \exp(-k_{\text{Au}^+} t)$  and  $\delta n_{\text{Au}^{3+}}^0 \exp(-k_{\text{Au}^{3+}} t)$ , respectively. Ignoring the thermal contribution in the long time range, we fitted the time profile of the TG signal in Fig. 2a by

$$I_{\text{TG}}(t) = A[\delta n_{\text{Au}^+}^0 \exp(-k_{\text{Au}^+} t) - \delta n_{\text{Au}^{3+}}^0 \exp(-k_{\text{Au}^{3+}} t)]^2. \quad (10)$$

Both the decay rate constants  $k_{\text{Au}^+}$  and  $k_{\text{Au}^{3+}}$  depend on the grating wavenumber  $q$ . Fig. 3a shows the  $q^2$  dependence of  $k_{\text{Au}^+}$  and  $k_{\text{Au}^{3+}}$ . Both rate constants show a good linear relationship with a negligibly small intercept with the ordinate axis. This linear relationship indicates that the rise and slower decay component is governed by the mass diffusion process in solutions. From the slope of each line and using the relation of  $k_i = D_i q^2$ , the diffusion coefficient of  $\text{Au}^+$  ( $D_{\text{Au}^+}$ ) and  $\text{Au}^{3+}$  ( $D_{\text{Au}^{3+}}$ ) are determined and shown later.

Interestingly, as shown in Fig. 2, b and c, the above rise and slow decay components disappeared after the photoirradiation by the mercury lamp within 1 min, while the thermal grating signal still remained. After the photoirradiation of 2 min, the TG signal appeared again, but it has two components, one is the slow decay with a lifetime of millisecond order and the other is much slower decay [25]. The signal intensity of this slower decay component should be due to the diffusion of Au particles, while millisecond-order decay component should be due to the diffusion of Au ionic species. Especially, as is shown in Fig. 2d, it was found that the slower decay signal originated from Au particle began to appear within 2 min before the slow decay signal originated from Au ionic species completely disappeared to the baseline level. It was also apparent that  $\text{Au}^{3+}$  species were consumed and  $\text{Au}^+$  species were produced during the short-duration photoirradiation (less than 3 min) [26]. This behavior may suggest that the reduction of  $\text{Au}^+$  to  $\text{Au}^0$  atoms and the association of  $\text{Au}^0$  atoms to form seed Au particle concurrently proceeds after all  $\text{Au}^{3+}$  are completely reduced to  $\text{Au}^+$ , which is consistent with our XAFS results [26].

After the photoirradiation by the mercury lamp for 5 min (Fig. 2, e and f), the TG signal was composed of three components; a slow decay with a decay rate constant less than ca. 1 ms, a slower rise with a decay rate constant around 40 ms, and a much slower decay with a decay rate constant longer than 100 ms. This feature was also observed in the longer reduction time, as shown in Fig. 2, k and l. It was obvious from these figures that the slowest decay signal intensity became stronger in the longer photoirradiation time.

The origins of these components were determined based on the following grounds. First, it should be noted that the decay rate constant of the initial decay was similar to that of the decay

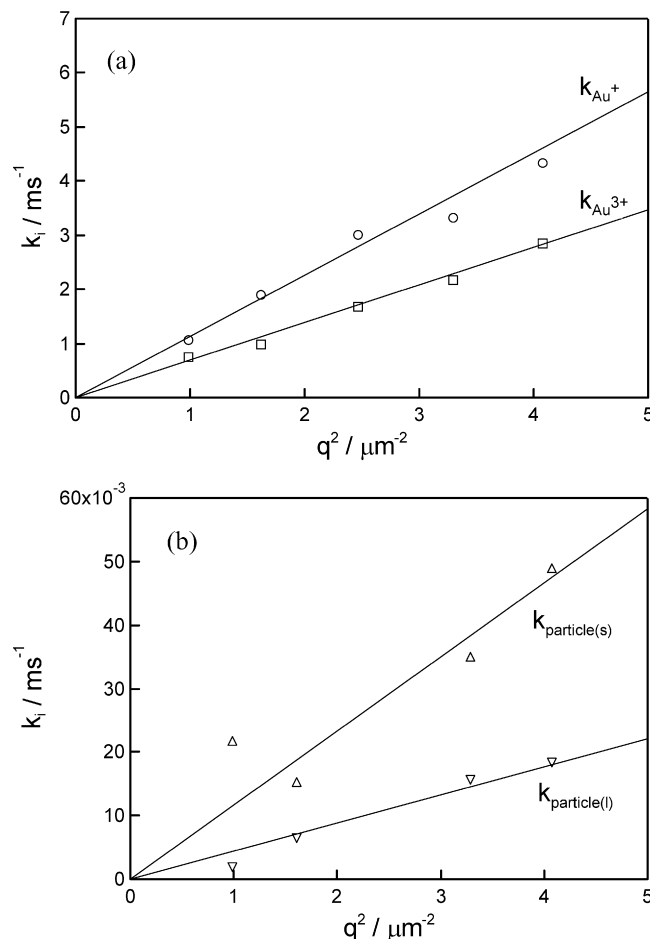


**Fig. 3.** Plot of the decay rate constants ( $k_i$ ) vs  $q^2$  of (a) chemical species ( $\square$ ,  $\text{Au}^{3+}$  and  $\circ$ ,  $\text{Au}^+$ ) existing before photoirradiation and (b) smaller and larger Au particles ( $\triangle$  and  $\nabla$ ) after the photoirradiation of 90 min in the 1:1 mixture solution of water and ethanol containing PVP. The concentration of polymer was at (a) [PVP monomeric unit]/[metal] = 4 (the dilute PVP solution) and (b) [PVP monomeric unit]/[metal] = 400 (the concentrated PVP solution).

component observed for shorter photoirradiation time, e.g., Fig. 2, d or e, which was attributed to the diffusion of  $\text{Au}^+$ . Hence, it is reasonable to consider that the initial decay is due to the diffusion of  $\text{Au}^+$ . Since there is no absorption of  $\text{Au}^+$  at the probe wavelength (633 nm), as shown in Fig. 1c, this component is due to the refractive index change. Second, the decay rate constant of the rise and slowest decay components were much larger than that of the  $\text{Au}^+$  component. This fact indicates that the chemical species contributing to these components should be much larger in size. Furthermore, it is already known that Au particles are formed after the photoirradiation of the  $\text{Au}^{3+}$  solutions [26]. Hence we attribute these rise-decay components to the Au particles. Here we should note that a tail of the broad plasmon absorption (maximum at the wavelength of 550 nm) due to the Au particles, produced by the photoirradiation for 15 min or longer-duration, is observed at the probe wavelength of 633 nm (Figs. 1a and 1b). The tail of the broad plasmon absorption is due to the larger contribution of light scattering effect than that of the plasmon absorption [31], since the present Au colloidal solution has a broad particle size distribution and contains some particles or aggregates larger than 10 nm (see TEM image shown in Fig. 7). If there is an absorption (light scattering) change ( $\delta k$ -term) nearly at the probe wavelength, in general, the amplitude change contributes to the TG signal more than the refractive index change [32]. Hence we consider that the dominant component of the species grating in the longer time range is due

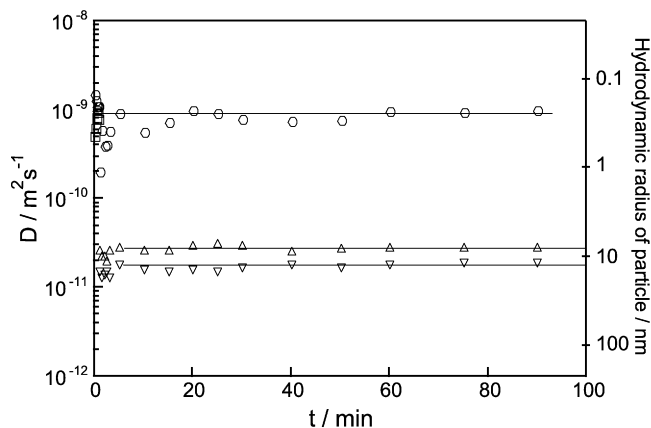


**Fig. 4.** Time evolution of  $D$  of four components produced during the photoirradiation; ( $\square$ )  $\text{Au}^{3+}$  ionic species, ( $\circ$ )  $\text{Au}^+$  ionic species, and ( $\Delta$ ,  $\nabla$ ) Au particles. Two components of the smaller and the larger Au particles are observed because the smaller particles were produced by the photofragmentation of the larger particles by the irradiation of excimer laser in water/ethanol (1/1) solutions in the TG measurements. The concentration of polymer was at  $[\text{PVP monomeric unit}]/[\text{metal}] = 4$  (the dilute PVP solution). The representative values of the hydrodynamic radius  $r$  are also indicated in the Y axis of the right side.

to the amplitude grating due to the Au particles. In this case, why did we observe rise-decay feature? Only one possible explanation which we can consider is that there are two types of Au particles with different diameters (smaller and larger) and the signs of the absorption changes (amplitude change) of these species are opposite. The larger Au particles should be photofragmented to some smaller Au particles by the excimer laser beam of the excimer laser which was used for creating TG signal. The origins of the smaller and larger Au particles will be discussed later.

Considering the photofragmentation of larger Au particles to smaller ones by the excimer laser as well as the consumption of  $\text{Au}^+$  species to proceed the subsequent reduction, the smaller particles are the product which should have a positive sign of  $\delta k_{\text{particle}(s)}^0$ , the larger particles are the reactant with a negative sign of  $\delta k_{\text{particle}(l)}^0$ , and the sign of  $\delta n_{\text{Au}^+}$  is negative. Therefore, on the basis of Eq. (8), the TG signal ( $I_{\text{TG}}(t)$ ) after photoirradiation is predicted to be expressed by

$$I_{\text{TG}}(t) = A[-\delta n_{\text{Au}^+}^0 \exp(-k_{\text{Au}^+} t)]^2 + B[\delta k_{\text{particle}(s)}^0 \exp(-k_{\text{particle}(s)} t) - \delta k_{\text{particle}(l)}^0 \exp(-k_{\text{particle}(l)} t)]^2, \quad (11)$$

where  $k_{\text{particle}(s)}$  and  $k_{\text{particle}(l)}$  is the decay rate constant of smaller and larger Au particles, respectively. The fact that the decay signal intensity with the decay rate constant longer than 100 ms became stronger with increasing the photoirradiation time, as shown in Fig. 2, can be explained in terms of the increase of the number of the larger Au particles with the photoirradiation time. The  $k_{\text{Au}^+}$ ,  $k_{\text{particle}(s)}$ , and  $k_{\text{particle}(l)}$  values were plotted against  $q^2$  in Figs. 3a and 3b. These plots show a good linear relationship and have near zero intercepts within the error (10% at most). From the slope of each line and using the relation of  $k_i = D_i q^2$ ,  $D_{\text{Au}^+}$ , a diffusion coefficient of smaller Au particles ( $D_{\text{particle}(s)}$ ), and that of larger Au particles ( $D_{\text{particle}(l)}$ ) are determined. The best-fitted curves by three components expressed by Eq. (11) are also shown in Fig. 2, f, h, j, and l.

Fig. 4 shows the time dependence of  $D$  plotted against the reduction time for the dilute PVP solution. As mentioned above, four chemical species are observed during the photoirradiation. The  $D$  values of  $\text{Au}^+$  remain constant ( $D_{\text{Au}^+} = 9.0 \times 10^{-10} \text{ m}^2/\text{s}$ ) within experimental error even in increasing the reduction time. The sig-

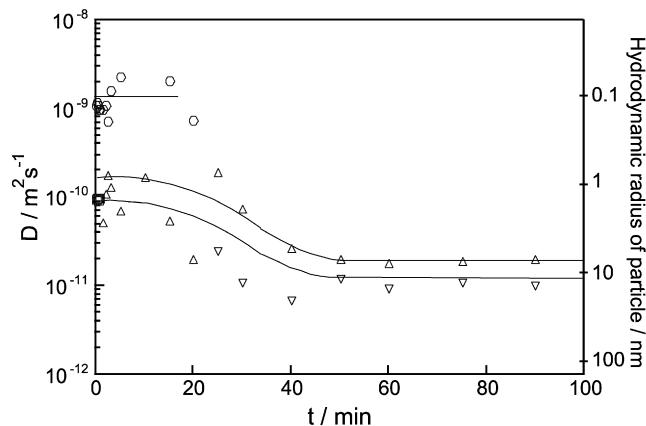


**Fig. 5.** Time evolution of  $D$  of four components produced during the photoirradiation of the concentrated PVP solution ( $[\text{PVP monomeric unit}]/[\text{metal}] = 400$ ); ( $\square$ )  $\text{Au}^{3+}$  ionic species, ( $\circ$ )  $\text{Au}^+$  ionic species, and ( $\Delta$ ,  $\nabla$ ) Au particles. As is seen in the case of the dilute PVP solution (Fig. 4), Au particles have two components due to the photofragmentation of the larger Au particles by the irradiation of excimer laser in water/ethanol (1/1) solutions in the TG measurements. The representative values of the hydrodynamic radius  $r$  are also indicated in the Y axis of the right side.

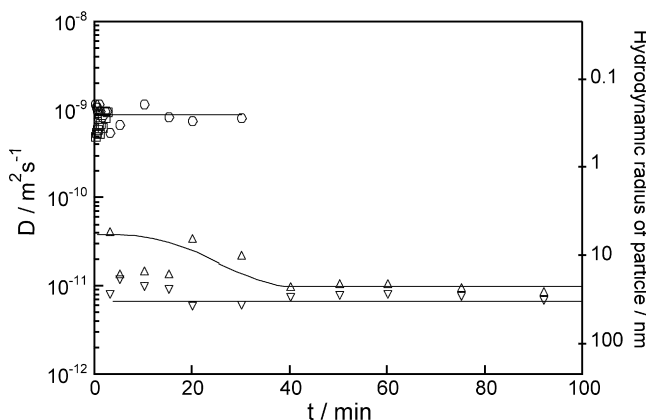


**Fig. 6.** Time evolution of  $D$  of four components produced during the photoirradiation of water/ethanol (1/1) solutions without PVP; ( $\square$ )  $\text{Au}^{3+}$  ionic species, ( $\circ$ )  $\text{Au}^+$  ionic species, and ( $\Delta$ ,  $\nabla$ ) Au particles. Au particles have two components due to the photofragmentation of the larger Au particles by the irradiation of excimer laser. The representative values of the hydrodynamic radius  $r$  are also indicated in the Y axis of the right side.

nal due to  $\text{Au}^{3+}$  can not be detected after at least 1 min reduction. The two contributions of the  $D$  values of the smaller and larger Au particles are constant ( $D_{\text{particle}(s)} = 2.9 \times 10^{-11} \text{ m}^2/\text{s}$  and  $D_{\text{particle}(l)} = 1.8 \times 10^{-11} \text{ m}^2/\text{s}$ , respectively). The details will be discussed later.

#### 4.2. Size of Au particles during photoreduction of $\text{AuCl}_4^-$

In order to investigate the effect of the protective polymer PVP, we tested other two different polymer concentrations, one is a concentrated PVP solution and the other is a solution without PVP. Figs. 5 and 6 show the time dependence of  $D$  plotted against the reduction time for the concentrated PVP solution and the Au solution without PVP, respectively, to compare with the dilute PVP solution (Fig. 4). The time evolution of the TG signals of the solution without PVP (not shown in this manuscript) was very similar to that with PVP except the intensity and the decay rate of the species grating.

In the case of the concentrated PVP solution (Fig. 5),  $D_{\text{Au}^+}$  is constant ( $1.3 \times 10^{-9} \text{ m}^2/\text{s}$ ) within experimental error. On the other hand,  $D_{\text{particle}(s)}$  and  $D_{\text{particle}(l)}$  are changed from  $1.7 \times 10^{-10} \text{ m}^2/\text{s}$  to  $2.0 \times 10^{-11} \text{ m}^2/\text{s}$  and from  $9.0 \times 10^{-11} \text{ m}^2/\text{s}$  to

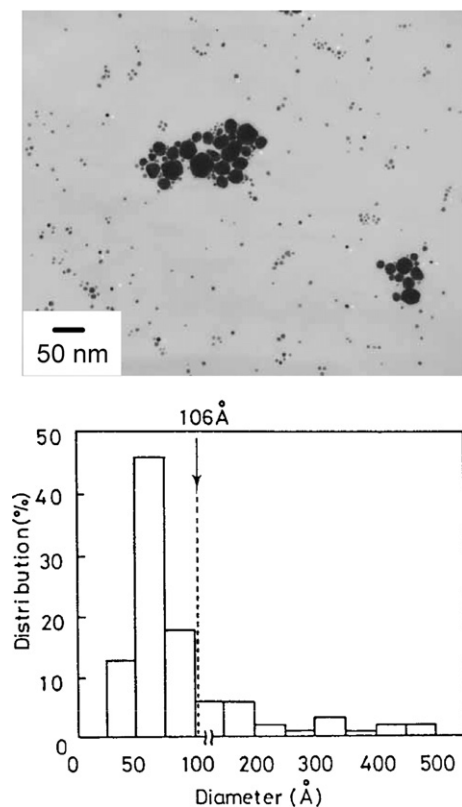


**Fig. 7.** TEM image and distribution of the diameter extracted from the corresponding image for the Au particles produced in the PVP solution by the photoirradiation for 120 min. 1:1 mixture of water and ethanol was used as a solvent. The concentration of polymer was at  $[\text{PVP monomeric unit}]/[\text{metal}] = 40$ .

$1.2 \times 10^{-11} \text{ m}^2/\text{s}$ , respectively, with the increase of the reduction time. Comparing the behavior for  $D_{\text{particle(s)}}$  and  $D_{\text{particle(l)}}$  in Fig. 4 with those in Fig. 5, it is noteworthy that  $D_{\text{particle(s)}}$  and  $D_{\text{particle(l)}}$  do not significantly change during the photoirradiation in the dilute PVP solution although these values gradually decrease in the concentrated PVP solution. At the reduction time of 90 min,  $D_{\text{particle(s)}}$  and  $D_{\text{particle(l)}}$  in the concentrated solution is close to those in the dilute solution. This indicates that the size of smaller and larger Au particles in the concentrated solution is nearly the same as in the dilute solution.

On the other hand, for the Au ionic solution without PVP (Fig. 6),  $D_{\text{Au}^+}$  is nearly equal to  $9.0 \times 10^{-10} \text{ m}^2/\text{s}$  and  $D_{\text{particle(s)}}$  and  $D_{\text{particle(l)}}$  become gradually close to the values of  $1.0 \times 10^{-11} \text{ m}^2/\text{s}$  and  $7.0 \times 10^{-12} \text{ m}^2/\text{s}$ , respectively, in the reduction time longer than 40 min. In particular,  $D_{\text{particle(s)}}$  decreases in the reduction time till 40 min. Here we find that  $D_{\text{particle(s)}}$  and  $D_{\text{particle(l)}}$  in solution without PVP is smaller than the corresponding value in other two cases.  $D_{\text{Au}^+}$  and  $D_{\text{Au}^{3+}}$  are nearly the same both in the dilute PVP solution and the solution without PVP. In the solution without PVP, large aggregates dispersed in solutions were observed during the photoreduction of  $\text{Au}^{3+}$  ions. However, TG measurements did not detect the aggregates because the decay time of these aggregates are not covered in the present experiments. Furthermore, the precipitation of Au particles was observed when the sample solution was kept under the ambient conditions for a couple of days. This implies that PVP works as a stabilizer in the clustering of atoms to produce their particles.

Fig. 7 shows the TEM image and size distribution of Au particles produced in the PVP solution (1:1 mixed solution of water and ethanol) by the photoirradiation of 120 min. As is shown in the image, the size distribution of particle diameter is relatively broad and has a long tail out to 50 nm, and some particles (or ag-

gregates) larger than 10 nm are observed. The average diameter is determined as 10.6 nm.

According to the Stokes–Einstein relationship,  $D$  of a spherical molecule having a radius  $r$  in a homogeneous nonviscous solvent with viscosity  $\eta$  is given by

$$D = kT/6\pi\eta r. \quad (12)$$

From  $D$  of the Au particles in the dilute PVP solution,  $r$  is calculated from the Eq. (12) to be 7.7 nm (for the smaller Au particle) and 12.3 nm (for the larger Au particle) on the basis of Stokes–Einstein relationship, respectively, as shown in Fig. 4. The histogram of the diameters of Au particles prepared in the dilute PVP solution from the TEM image (broader size distribution as shown in Fig. 7) do not coincide with that expected from  $D_{\text{particle(s)}}$  and  $D_{\text{particle(l)}}$  of the Au particles ( $2r = 15.4 \text{ nm}$  for the smaller and  $2r = 24.6 \text{ nm}$  for the larger Au particles, respectively). The radius from the TEM observation corresponds to the size of the metallic cores, but it does not include a polymer layer adsorbed on the surface of the particles. On the other hand, in the case of the concentrated PVP solution,  $2r$  is calculated to be 13.9 nm (for the smaller particle) and 23.1 nm (for the larger particle). Additionally, in the case of the solutions without PVP,  $2r$  is calculated to be 44.4 nm (for the smaller particle) and 63.4 nm (for the larger particle). The particle sizes of the smaller and larger Au particles in the dilute solutions are slightly larger than those in the concentrated solutions, but the particle sizes in the solutions without PVP are much larger than those in the dilute solutions. In the solutions without PVP, the created particles became to form precipitates under the ambient conditions for a couple of days.

#### 4.3. Laser-induced photofragmentation of Au particles in polymer solutions

According to the investigation of Koda et al. [33], laser-induced size reduction of Au particles was observed in aqueous solution by means of the irradiation of a pulsed Nd:YAG laser. They reported that the Au particles possessing a diameter larger than ca. 20 nm were transformed to the smaller particles less than ca. 10 nm by the laser-irradiation. If the size reduction mechanism is applied to the present Au colloidal solutions, larger Au particles produced by the photoirradiation of the mercury lamp would be photofragmented to small Au particles by the excitation beam of the excimer laser during the TG measurement. In other words, larger Au particles (20–25 nm in diameter estimated from the present TG measurements), whose diameter must exceed a threshold value (the expected threshold value of ca. 20 nm as likely as in Ref. [33]), should be photofragmented to small Au particles (13–16 nm in diameter estimated from TG) by the excitation beam of an excimer laser.

It should be noted that the irradiated volume by the excimer laser is very little in the sample solution during the TG measurements because of its small beam size, and the irradiation using the excimer laser is performed just during the TG measurements. Hence, little amount of the Au particles is photofragmented to small Au particles by the excimer laser and, on the contrary, most of all the Au particles are produced by the photoirradiation using the mercury lamp. Therefore, the photofragmented small Au particles are transient species during the TG measurements, and the larger Au particles really exist in the particle growth process and their particle growth is significantly controlled by the photoirradiation using the mercury lamp, not by the excimer laser. Hereafter we shall focus on the larger Au particles produced from the photoirradiation by the mercury lamp.

First we shall consider the particle growth mechanism in the PVP solution by the careful observation of the TG signal intensities since the process of Au particle growth is very complicated.

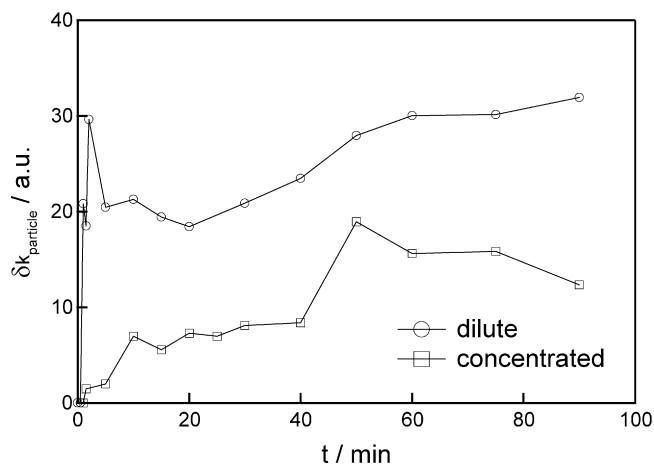


**Fig. 8.** Plot of the species grating intensity of the larger Au particles ( $\delta k_{\text{particle}(l)}$ ) produced by the photoirradiation of the mercury lamp against the reduction time. The concentration of polymer was as follows, (○) the dilute PVP solution ([PVP monomeric unit]/[metal] = 4) and (□) the concentrated PVP solution ([PVP monomeric unit]/[metal] = 400).

**Fig. 8** shows the time evolution of the TG signal intensities due to the larger Au particles ( $\delta k_{\text{particle}(l)}$ ) in the fitting with Eq. (11) for the dilute and the concentrated PVP solutions against reduction time. In the case of the dilute PVP solution, the TG signal intensity drastically increases after 1 min of the photoirradiation and is almost saturated within 10 min. On the successive photoirradiation over 10 min, gradual increase of signal intensity is observed with the increase of the reduction time, indicating that the samples photoirradiated for longer time show the photofragmentation of the larger Au particles (with  $D_{\text{particle}(l)}$ ) occurs to the same extent in the colloidal solution. On the contrary,  $\text{Au}^+$  species still remain in the solution and they might be continuously reduced to  $\text{Au}^0$  atoms by the photoirradiation on the existing smaller Au particles (whose diameters are less than those of the larger Au particles). This autocatalytic growth process [34–36] occurs during the photoirradiation and finally their particle size approaches to the uniform size, which is representative of larger Au particles, in course of reduction time.

On the other hand, in the case of the concentrated PVP solution, the TG signal intensity increases more slowly during the first 40 min, and then gradually increases in time till 90 min. In the short-duration photoirradiation (0–10 min), especially, the values of  $\delta k_{\text{particle}(l)}$  are smaller in the concentrated PVP solution than those in the dilute one. The slower production of larger Au particles in the concentrated solution than in the dilute solution indicates that polymer concentration would affect the rate of particle growth due to the interactions between the polymer chains and Au particles (or Au ions). These interactions might suppress the rate of particle growth more noticeably as the size of Au particles becomes larger and larger.

#### 4.4. Time evolution of Au particle formation and comparison with Pt particle formation

**Fig. 9** illustrates the Au particle formation schemes in PVP solution during the photoreduction using the mercury lamp from  $\text{AuCl}_4^-$  to Au particles. **Fig. 9a** presents the ionic precursor of  $\text{AuCl}_4^-$  in the solution before the photoirradiation. Once the photoirradiation is performed, the rapid reduction of  $\text{AuCl}_4^-$  to  $\text{AuCl}_2^-$  occurs (**Figs. 9b and 9c**) and chemically-stable  $\text{AuCl}_2^-$  exists in the solutions (**Fig. 9c**). The reduction of  $\text{AuCl}_4^-$  is concomitant with the formation of Au particles (as shown in **Figs. 9c and 9d**). The transformation of  $\text{AuCl}_4^-$  to  $\text{AuCl}_2^-$  completes within 1 min, which corresponds to the route from the spectrum of **Fig. 2**, a to c. After

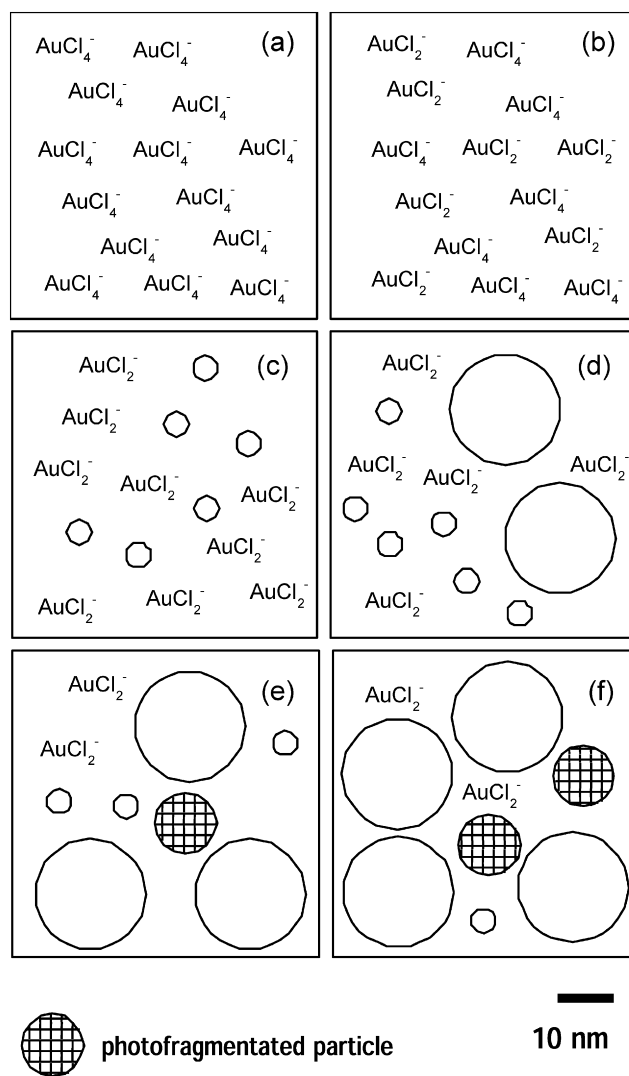


**Fig. 9.** Schematic illustration of the photoreduction process of the Au-containing solution (ethanol–water, 1:1 (v/v)) (a) before and (b–f) after the long-duration photoirradiation. Panels (a) to (d): These illustrations represent the state of the Au ionic species as well as the Au particles at the photoirradiation process. Panels (e) and (f): On the irradiation by an excimer laser, the photofragmentation of larger Au particles (ca. 20–25 nm expected from  $D_{\text{particle}(l)}$ ) occurs in the colloidal solutions, resulting in the formation of the small amount of the photofragmentated Au particles (ca. 13–16 nm expected from  $D_{\text{particle}(s)}$ ).

the irradiation of 5 min, only  $\text{AuCl}_2^-$  exists in the solution containing Au particles shown in **Fig. 9d**. It is obvious that  $\text{AuCl}_2^-$  is much more stable than  $\text{AuCl}_4^-$  in the aqueous solution under the long-duration photoirradiation. **Figs. 9e and 9f** show the schematic illustration of the small area irradiated by an excimer laser. During the long-duration photoirradiation using mercury lamp, the stable  $\text{AuCl}_2^-$  remains and the number of larger Au particles (ca. 20–25 nm expected from  $D_{\text{particle}(l)}$ ) increases in reduction time (the process from **Fig. 9d** to **9e**) even after the irradiation by the excimer laser. The photofragmentation of the larger Au particles is more remarkably induced by the excitation from the excimer laser because of the increasing number of larger Au particles, resulting in the number of smaller photofragmentated Au particles (ca. 13–16 nm expected from  $D_{\text{particle}(s)}$ ) increases accordingly, as shown in **Fig. 9f**. For the much longer reduction time, increase of the number of the larger Au particles might be observed owing to the reduction of the remaining  $\text{Au}^+$  on the surface of Au particle (with a diameter less than that of the larger Au particles) via the autocatalytic particle growth.

In our recent study [25,37], we investigated the photoreduction process of  $\text{PtCl}_6^{2-}$  to Pt particles during photoirradiation by means of the TG measurements. Upon photoirradiation to the  $\text{PtCl}_6^{2-}$  solution, the species grating signal due to  $\text{PtCl}_6^{2-}$  diminished and then the TG signal of Pt particles gradually appeared. This result indicates that the gradual clustering of Pt<sup>0</sup> atoms into Pt particles occurs after all  $\text{PtCl}_6^{2-}$  ions are photochemically reduced to  $\text{PtCl}_4^{2-}$  and subsequently transformed to Pt<sup>0</sup> atoms with a short delay. However, in the  $\text{AuCl}_4^-$  solution, the rapid reduction of  $\text{AuCl}_4^-$  to  $\text{AuCl}_2^-$  occurred, and the subsequent reduction of  $\text{AuCl}_2^-$  to Au<sup>0</sup> atoms is concomitant with the formation and growth of Au metal particles [26]. The formation of larger Au particles, which are produced during the short-duration photoirradiation (0–10 min), might be activated when the reduction of  $\text{AuCl}_2^-$  to Au<sup>0</sup> atoms proceed on the surface of the small Au particles (less than ca. 20 nm) via the autocatalytic particle growth.

## 5. Conclusion

The translational diffusion of Au ions and Au particles during the photoreduction process in aqueous ethanol solution of poly-(*N*-vinyl-2-pyrrolidone) (PVP) was investigated by using UV–vis absorption and the laser induced transient grating (TG) methods. The diffusion coefficients (*D*) of the Au ionic species and the Au particles during the photoreduction of  $\text{AuCl}_4^-$  were examined. The TG signal of  $\text{AuCl}_4^-$  solution before photoirradiation was composed of three contributions; the thermal grating, the species grating due to the creation of  $\text{AuCl}_2^-$ , and that due to the depletion of  $\text{AuCl}_4^-$ . The TG signal due to the diffusion of Au particles appears just after the TG signal due to  $\text{AuCl}_4^-$  disappeared and the transformation of  $\text{AuCl}_4^-$  to  $\text{AuCl}_2^-$  completed within 2 min. The reduction of  $\text{AuCl}_2^-$  is concomitant with the formation of Au particles in the short-duration photoirradiation (for example, 0–10 min in the case of the dilute PVP solution). When the particle size of the Au particles exceeds a threshold particle size (expected value of ca. 20 nm in diameter) in course of the photoirradiation time, two contributions are observed in TG signal coming from the two different diffusion coefficients ( $D_{\text{particle(s)}}$  and  $D_{\text{particle(l)}}$ ). One is the contribution due to the smaller Au particles (ca. 13–16 nm in diameter) produced from the photofragmentation of larger Au particles (ca. 20–25 nm in diameter) by excimer laser, and the other is due to larger Au particles themselves produced by the photoirradiation using the mercury lamp.

## Acknowledgments

We are grateful to the valuable discussions to Prof. H. Einaga at Department of Energy and Material Sciences, Faculty of Engineering Sciences, Kyushu University, Japan. One of the authors (K.O.) acknowledges support from JST PRESTO.

## References

- [1] (a) C.B. Murray, D.J. Norris, M.G. Bawendi, *J. Am. Chem. Soc.* 115 (1993) 8706; (b) H. Bönemann, R.M. Richards, *Eur. J. Inorg. Chem.* (2001) 2455.
- [2] (a) G. Schmid (Ed.), *Clusters and Colloids*, VCH, Weinheim, 1994; (b) G. Schmid, *Chem. Rev.* 92 (1992) 1709.
- [3] D.L. Feldheim, C.A. Foss Jr., *Metal Nanoparticles: Synthesis, Characterization, and Applications*, Marcel Dekker, New York, 2002.
- [4] E. Gachard, H. Remita, J. Khatouri, B. Keita, L. Nadjo, J. Belloni, *New J. Chem.* (1998) 1257.
- [5] (a) D.G. Duff, P.P. Edwards, B.F.G. Johnson, *J. Phys. Chem.* 99 (1995) 15934; (b) Y.-P. Sun, J.E. Riggs, H.W. Rollins, R. Guduru, *J. Phys. Chem. B* 103 (1999) 77; (c) M. Harada, N. Toshima, K. Yoshida, S. Isoda, *J. Colloid Interface Sci.* 283 (2005) 64.
- [6] (a) B.G. Ershov, A. Henglein, *J. Phys. Chem. B* 102 (1998) 10663; (b) B.G. Ershov, A. Henglein, *J. Phys. Chem. B* 102 (1998) 10667.
- [7] L. Bronstein, D. Chernyshov, P. Valetsy, N. Tkachenko, H. Lemmetyinen, J. Hartmann, S. Förster, *Langmuir* 15 (1999) 83.
- [8] (a) J. Tanori, T. Gulik-Krzywicki, M.P. Pileni, *Langmuir* 13 (1997) 632; (b) J. Tanori, M.P. Pileni, *Langmuir* 13 (1997) 639.
- [9] (a) R.L. Whetten, W.M. Gelbart, *J. Phys. Chem.* 98 (1994) 3544; (b) D.V. Leff, P.C. Ohara, J.R. Heath, W.M. Gelbart, *J. Phys. Chem.* 99 (1995) 7036.
- [10] (a) M. Zhao, L. Sun, R.M. Crooks, *J. Am. Chem. Soc.* 120 (1998) 4877; (b) M. Zhao, R.M. Crooks, *Angew. Chem. Int. Ed.* 38 (1999) 364.
- [11] (a) M. Brust, M. Walker, D. Bethell, D.J. Schiffrin, R. Whyman, *J. Chem. Soc. Chem. Commun.* (1994) 801; (b) A.C. Templeton, W.P. Wuelfing, R.W. Murray, *Acc. Chem. Res.* 33 (2000) 27.
- [12] (a) L.O. Brown, J.E. Hutchison, *J. Am. Chem. Soc.* 121 (1999) 882; (b) J. Yang, J.Y. Lee, T.C. Deivaraj, H.P. Too, *J. Colloid Interface Sci.* 277 (2004) 95.
- [13] (a) N. Shirtcliffe, U. Nickel, S. Schneider, *J. Colloid Interface Sci.* 211 (1999) 122; (b) Y.W. Tsai, Y.L. Tseng, L.S. Sarma, D.G. Liu, J.F. Lee, B.J. Hwang, *J. Phys. Chem. B* 108 (2004) 8148.
- [14] (a) U. Nickel, A.Z. Castell, P. Karin, S. Schneider, *Langmuir* 16 (2000) 9087; (b) B. Veisz, Z. Kiraly, *Langmuir* 19 (2003) 4817.
- [15] (a) K. Okitsu, A. Yue, S. Tanabe, H. Matsumoto, Y. Yobiko, *Langmuir* 17 (2001) 7717; (b) K. Okitsu, A. Yue, S. Tanabe, H. Matsumoto, Y. Yobiko, Y. Yoo, *Bull. Chem. Soc. Jpn.* 75 (2002) 2289.
- [16] (a) M.T. Reetz, W. Helbig, *J. Am. Chem. Soc.* 116 (1994) 7401; (b) M.T. Reetz, W. Helbig, S.A. Quaiser, U. Stimming, N. Breuer, R. Vogel, *Science* 267 (1995) 367.
- [17] (a) K. Kurihara, J. Kizling, P. Stenius, J.H. Fendler, *J. Am. Chem. Soc.* 105 (1983) 2574; (b) K. Kurihara, J.H. Fendler, *J. Am. Chem. Soc.* 105 (1983) 6152.
- [18] (a) K. Torigoe, K. Esumi, *Langmuir* 8 (1992) 59; (b) A. Kameo, A. Suzuki, K. Torigoe, K. Esumi, *J. Colloid Interface Sci.* 241 (2001) 289; (c) H.H. Huang, X.P. Ni, G.L. Loy, C.H. Chew, K.L. Tan, F.C. Loh, J.F. Deng, G.Q. Xu, *Langmuir* 12 (1996) 909.
- [19] (a) H.J. Eichler, P. Günter, D.W. Pohl, *Laser Induced Dynamic Gratings*, Springer-Verlag, Berlin, 1986; (b) M.D. Fayer, *Annu. Rev. Phys. Chem.* 33 (1982) 63; (c) J.T. Fourkas, M.D. Fayer, *Acc. Chem. Res.* 25 (1992) 227.
- [20] (a) M. Terazima, N. Hirota, *J. Chem. Phys.* 98 (1993) 6257; (b) K. Okamoto, M. Terazima, N. Hirota, *J. Chem. Phys.* 103 (1995) 10445; (c) K. Okamoto, N. Hirota, M. Terazima, *J. Phys. Chem. A* 101 (1997) 5380; (d) K. Okamoto, N. Hirota, M. Terazima, *J. Phys. Chem. A* 102 (1998) 3447; (e) T. Okazaki, N. Hirota, M. Terazima, *J. Photochem. Photobiol. A Chem.* 99 (1996) 155.
- [21] L. Richard, L. Genberg, J. Deak, H.-L. Chiu, R.J.D. Miller, *Biochemistry* 31 (1992) 10703.
- [22] (a) T. Nada, M. Terazima, *Biophys. J.* 85 (2003) 1876; (b) S. Nishida, T. Nada, M. Terazima, *Biophys. J.* 87 (2004) 2663; (c) S. Nishida, T. Nada, M. Terazima, *Biophys. J.* 89 (2005) 2004; (d) T. Eitoku, Y. Nakasone, D. Matsuoka, S. Tokutomi, M. Terazima, *J. Am. Chem. Soc.* 127 (2005) 13238; (e) M. Terazima, *Acc. Chem. Res.* 33 (2000) 687.
- [23] (a) K. Jarasiunas, H.J. Gerritsen, *Appl. Phys. Lett.* 33 (1978) 190; (b) D.P. Norwood, H.-E. Swoboda, M.D. Dawson, A.L. Smirl, D.R. Andersen, T.C. Hasenberg, *Appl. Phys. Lett.* 59 (1991) 219; (c) D.S. McCallum, X.R. Huang, M.D. Dawson, T.F. Boggess, A.L. Smirl, T.C. Hasenberg, A. Kost, *J. Appl. Phys.* 71 (1992) 929.
- [24] K. Okamoto, A. Kaneta, K. Inoue, Y. Kawakami, M. Terazima, T. Mukai, G. Shinomiya, Sg. Fujita, *Phys. Status Solidi B* 228 (2001) 81.
- [25] M. Harada, K. Okamoto, M. Terazima, *Langmuir* 22 (2006) 9142.
- [26] M. Harada, H. Einaga, *Langmuir* 23 (2007) 6536.
- [27] M. Terazima, K. Okamoto, N. Hirota, *J. Phys. Chem.* 97 (1993) 5188.
- [28] O. Horvath, K.L. Stevenson, *Charge Transfer Photochemistry of Coordination Compounds*, VCH, New York, 1993.
- [29] (a) H. Hase, S. Arai, A. Isomura, N. Terazawa, Y. Miyatake, M. Hoshino, *J. Phys. Chem.* 100 (1996) 11534; (b) Y. Miyatake, H. Hase, T. Saito, M. Onishi, Y. Tajima, M. Hoshino, *J. Phys. Chem. B* 108 (2004) 2540.
- [30] K. Millick, Z.L. Wang, T. Pal, *J. Photochem. Photobiol. A Chem.* 140 (2001) 75.
- [31] K.L. Kelly, T.R. Jensen, A.A. Lazarides, G.C. Schatz, in: D.L. Feldheim, C.A. Foss Jr. (Eds.), *Metal Nanoparticles: Synthesis, Characterization, and Applications*, Marcel Dekker, New York, 2002, chap. 4.
- [32] K.A. Nelson, R. Casalegno, R.J.D. Miller, M.D. Fayer, *J. Chem. Phys.* 77 (1982) 1144.
- [33] A. Takami, H. Kurita, S. Koda, *J. Phys. Chem. B* 103 (1999) 1226.
- [34] A. Henglein, *Chem. Rev.* 89 (1989) 1861.
- [35] Z.-Y. Huang, G. Mills, B. Hajek, *J. Phys. Chem.* 97 (1993) 11542.
- [36] C.E. Hoppe, M. Lazzari, I. Pardinas-Blanco, M.A. Lopez-Quintela, *Langmuir* 22 (2006) 7027.
- [37] M. Harada, H. Einaga, *Langmuir* 22 (2006) 2371.